Key Points:
- N cycling plays an important role in affecting northern peatland radiative forcing
- Northern peatlands are estimated to accumulate 408 Pg C and 7.8 Pg N during 15 ka BP-1990
- Northern peatlands will have a weaker cooling effect in 2100 by 7%–79% primarily due to increasing CH_4 emissions

Author Contribution:
Conceptualization: Qianlai Zhuang
Funding acquisition: Qianlai Zhuang
Project administration: Qianlai Zhuang
Resources: Qianlai Zhuang
Supervision: Qianlai Zhuang
Writing – review & editing: Qianlai Zhuang

Nitrogen Cycling Feedback on Carbon Dynamics Leads to Greater CH_4 Emissions and Weaker Cooling Effect of Northern Peatlands

Bailu Zhao[1] and **Qianlai Zhuang[1,2]**

[1]Department of Earth, Atmospheric, and Planetary Sciences, Purdue University, West Lafayette, IN, USA, [2]Department of Agronomy, Purdue University, West Lafayette, IN, USA

Abstract Northern peatlands have been a carbon sink since their initiation. This has been simulated by existing process-based models. However, most of these models are limited by lacking sufficient processes of the N cycle in peatlands. Here, we use a peatland biogeochemistry model incorporated with N-related processes of fixation, deposition, gas emission, loss through water flow, net mineralization, plant uptake and litterfall to project the role of the peatlands in future radiative forcing (RF). Simulations from 15-ka BP to 2100 are conducted driven by CMIP5 climate forcing data of IPSL-CM5A-LR and bcc-csm1-1, including warming scenarios of RCP 2.6, RCP 4.5 and RCP 8.5. During the Holocene, northern peatlands have an increasing cooling effect with RF up to -0.57 W m^{-2}. By 1990, these peatlands accumulate 408 Pg C and 7.8 Pg N. Under warming, increasing mineral N content enhances plant net primary productivity; the cooling effect persists. However, RF increases by 0.1–0.5 W m^{-2} during the 21st century, mainly due to the stimulated CH_4 emissions. Northern peatlands could switch from a C sink to a source when the annual temperature exceeds -2.2 to -0.5°C. This study highlights that the improved N cycle causes higher CO_2-C sink capacity in northern peatlands. However, it also causes a significant increase in CH_4 emissions, which weakens the cooling effect of northern peatlands in future climate.

Plain Language Summary This study develops a process-based model, the Peatland Terrestrial Ecosystem Model, by considering how peatland N cycling influences C cycling. The model estimates the northern peatland C and N dynamics during 15ka BP to 2100. By 1990, northern peatlands have accumulated 408 Pg C and 7.8 Pg N, with an increasing cooling effect during 15ka BP-1990. During the 21st century, northern peatlands will continue to have a cooling effect on climate. It will weaken due to increased greenhouse gas (GHG) emissions, especially CH_4. This study highlights the role of the N cycle in the C dynamics of northern peatlands and emphasizes the importance of CH_4 emissions in future northern peatlands carbon-climate feedback.

1. Introduction

Peatlands have less than 3% of global land coverage, mainly in northern high latitudes (>45°N) (Xu et al., 2018). Despite the low coverage, C storage in northern peatlands is estimated to be 450 ± 100 Pg C (Hugelius et al., 2020; Spahni et al., 2013) due to high C content on a unit area. Carbon in northern peatlands is stored in the soil organic layer, which can be a few meters in depth (Loisel et al., 2014). Soil organic matter accumulates under cold and wet conditions where the anoxic environment slows down the rate of dead plant decomposition (Finlayson & Milton, 2018). Most of the northern peatlands were initiated after 12 ka BP and have been acting as a C sink since their initiation (Gorham et al., 2007).

In the future, the northern high latitudes are likely to experience a more severe warming than the other parts of the Earth (Rantanen et al., 2022). This change in climate may interrupt the long-lasting pattern of C accumulation of northern peatlands. The direct influences of warming include the increase of both productivity and microbial activity (i.e., decomposition rates), indicating more intensive C sequestration and releasing (Hanson et al., 2020; Richardson et al., 2018). Warming also enhances peat decomposition indirectly via drought and permafrost thaw, where the former switches partial soil C from anaerobic to aerobic conditions and the latter releases previously frozen peat for decomposition (Finger Higgens et al., 2019; Frolking et al., 2011; Gallego-Sala et al., 2018; Huang et al., 2021). In addition, fires and human-derived land use changes are likely to release significant amounts of C into the atmosphere (Loisel et al., 2021). Under these conditions, northern peatlands are projected to be a weaker
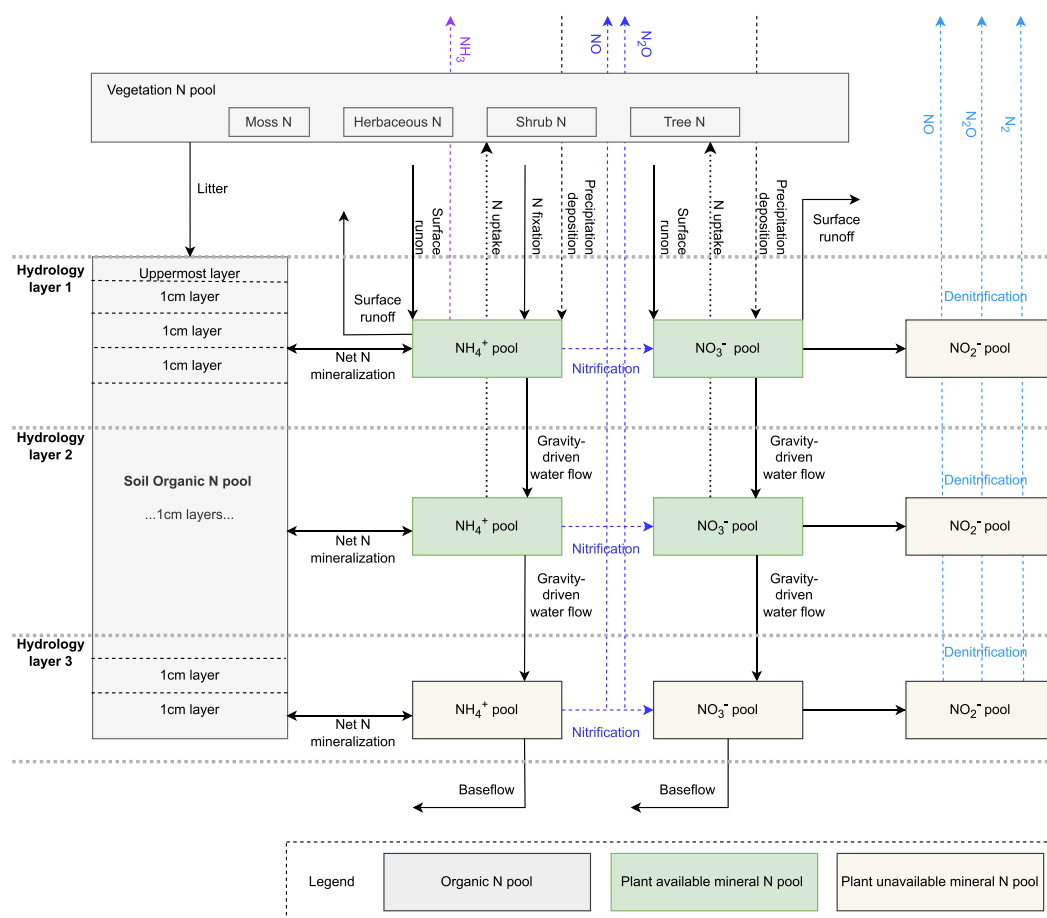
Figure 1. The N cycle in PTEM 2.3.

C sink or switch to a C source by the end of the 21st century (Chaudhary et al., 2020; Spahni et al., 2013; Zhao & Zhuang, 2023a).

These projections of northern peatlands are made using process-based models such as LPX-Bern 1.0 (Land surface Processes and eXchanges model Bern version) (Spahni et al., 2013), ORCHIDEE-PEAT (Organizing Carbon and Hydrology In Dynamic Ecosystems, peatland version) (Qiu et al., 2021), LPJ-GUESS (Lund-Potsdam-Jena General Ecosystem Simulator) (Chaudhary et al., 2017), HPM (Holocene Peatland Model) (Treat et al., 2021) and PTEM 2.2 (Peatland Terrestrial Ecosystem Model) (Zhao & Zhuang, 2023a). However, one common source of uncertainty of these models is the lack of a complete nitrogen cycle (Frolking et al., 2010; Spahni et al., 2013; Zhao & Zhuang, 2023a). For example, LPX-Bern 1.0 has included atmospheric N deposition and other N inputs, vegetation N uptake, litterfall N and N mineralization (Spahni et al., 2013). PTEM 2.2 includes the same processes as LPX-Bern 1.0, and also considers the N loss from water runoff (Zhao & Zhuang, 2023a). These models are unable to track nitrification, denitrification, biological N fixation (BNF) and N gas loss, and a mineral N pool is missing. Although a DyN (the global Dynamic Nitrogen) model is developed based on the LPJ-DGVM (Lund-Potsdam-Jena Model Dynamic Global Vegetation Model) framework and considers these N-related processes missing in current peatland models, DyN is not designed to describe peatland biogeochemical processes and was not applied to peatlands simulation (Xu & Prentice, 2008). Notably, higher N availability could increase the productivity of woody plants, reduce that of Sphagnum, and increase the decomposition rate of northern peatlands. With a lower N availability, the opposite trend is found (Gunnarsson & Rydin, 2000; Ojanen et al., 2019; Song et al., 2018). With the incomplete N cycle, current peatland models are limited in quantifying the past and future C budgets.

To address this knowledge gap, we embedded a complete N cycle to PTEM 2.2 and created an updated PTEM 2.3 (Figure 1). A simulation from 15 ka BP to 2100 was conducted with the revised model. The following questions

are answered: (a) how did northern peatlands accumulate C and N during the Holocene (15 ka BP-1990)? (b) How will northern peatlands C and N fluxes and stocks respond to future climate change? (c) What is the threshold temperature and precipitation for a pan-Arctic sink and source shift? (d) How are the C and N stocks, fluxes and thresholds different from the simulation without a complete N cycle?

2. Methods

2.1. PTEM 2.2 Overview

PTEM 2.2 is a version of the Terrestrial Ecosystem Model incorporated with the biogeochemical processes of northern peatlands. PTEM 2.2 runs simulations on a monthly time step, and there are four plant functional types (PFTs) considered: moss, herbaceous, shrubs and trees (Zhao & Zhuang, 2023a). In each month, the C sequestrated by the ecosystem is allocated into four PFTs according to their relevant dominance, which is influenced by water table depth (WTD), N availability and the PFT's current plant C. In addition, the productivity of moss is also influenced negatively by the coverage of vascular plants due to the shadowing effect (Zhao, Zhuang, Treat, & Frolking, 2022). In each month, a PFT-specific fraction of plant C and N falls as litter and becomes input to soil organic C and N pools. The soil C pool is divided into 1 cm layers. The bulk density, C density, fraction of remaining original litter, and the C content of each layer are calculated. The bulk density of relatively undecomposed peat is lower. With decomposition, the fraction of original peat decreases, and the bulk density increases.

PTEM 2.2 simulates both aerobic and anaerobic decomposition. When the soil layer is not saturated, the decomposition is aerobic and produces CO_2. Otherwise, the decomposition is mainly anaerobic, and produces mostly CH_4 with limited amounts of CO_2. PTEM 2.2 has a soil thermal module keeping track of the changes in active layer depth (ALD). When the soil layer is frozen, there is no decomposition (Zhao, Zhuang, Treat, & Frolking, 2022). Different from soil C, the soil organic N pool in PTEM 2.2 is not divided into layers. The plant-available N comes from rainfall, run-on and net N mineralization, while available N loss pathways are vegetation N uptake and N outflow (Zhao, Zhuang, Treat, & Frolking, 2022). In particular, the net N mineralization rate is influenced by the soil C:N ratio and the intensity of microbial activity (surrogated by the soil C decomposition rate).

PTEM 2.2 simulation is composed of two steps: WTD simulation and peat simulation. In the WTD simulation, PTEM 2.2 estimates the WTD of the entire grid cell ($0.5° \times 0.5°$). Each grid cell is then divided into 100 sub-grid cell bins with topographic wetness index (TWI) values. As an index showing the likelihood of water flowing into the area of interest, higher TWI values correspond to higher probability of flooding and shallower WTD. Thereafter, the WTD in each bin can be estimated by the grid-cell average WTD and the bin-specific TWI via a TOPMODEL approach. The interpolated WTD is used as the input for peat simulation for four purposes: (a) determining the boundary of aerobic and anaerobic decomposition; (b) estimating soil moisture; (c) calculating the amount of run off and baseflow which carry away N; (d) adding additional run-on with dissolved mineral N when the precipitation alone is not sufficient to maintain the input WTD (Zhao & Zhuang, 2023a). After the peat simulation, the peatland area is calculated by counting the number of bins with long-term WTD shallower than 25 cm and peat thickness higher than 30 cm.

The N cycle influences the C cycle in PTEM 2.2 with two key carbon fluxes: net primary productivity (NPP) and decomposition. In each month, NPP is computed for each PFT. The N limit on NPP is calculated by the C:N ratio of PFT. When the plant C:N ratio reaches the PFT-specific maximum, there is no sufficient N to support additional C assimilation, thereby NPP is the lowest. On the contrary, when the plant C:N ratio reaches the PFT-specific minimum, NPP is the highest. The C:N ratio is not only determined by the C and N amount in the existing plant tissue but also by the amount of N uptake by the plants in the current month. Therefore, even if the C:N ratio in the existing plant tissue reaches the PFT's maximum, the plants can still assimilate C by additional N uptake. The rate of PFT N uptake is influenced by the amount of available mineral N in the soil. In terms of decomposition, PTEM has PFT-specific decomposition rates at 0°C as the key parameter. These parameters are influenced by the C:N ratio of the litter, that is, the plant C:N ratio by the end of the growing season. When N is insufficient and the ratio is higher, there is a lower decomposition rate.

2.2. Revisions to PTEM 2.2

The existing N flows in PTEM 2.2 include mineralization, run-on/run-off, vegetation N uptake and N litterfall. On top of the existing N flows, PTEM 2.3 adds nitrification, denitrification, N flow via vertical water flow, gas emission, N fixation, and N deposition (Figure 1).

The N pool in PTEM 2.2 is divided into PFT vegetation N pools, the soil organic N pool and the mineral N pool. This structure remains the same in PTEM 2.3 but with finer divisions. In particular, the mineral N pool is divided into three layers following the hydrology structure of PTEM 2.3. In each layer, the organic and mineral N are interconvertible via mineralization and immobilization. The direction of interconversion is primarily controlled by the soil C:N ratio, such that both mineral and organic pools are not depleted. In each layer, the mineral N pool is further divided into NH_4^+, NO_3^- and NO_2^- pools (Figure 1). The NH_4^+ and NO_3^- pools in the top two hydrology layers compose the available N pool. In each month, each PFT uptakes N from the available N pool. In PTEM 2.3, the algorithms of how N limits NPP and affects decomposition remain the same as PTEM 2.2. The details of model revision are provided in Text S1 in Supporting Information S1. Same as PTEM 2.1 (Zhao, Zhuang, & Frolking, 2022), PTEM 2.3 requires spatially explicit peat initiation input. The peat thickness, soil organic C stock and soil organic N stock all start as 0 in the year of peat initiation. An equilibrium run is conducted before transient simulation. The model flux variables usually stabilize after decades of simulation, which is very short compared with the total simulation period (usually thousands of years). Compared with previous versions, the revised PTEM 2.3 can estimate (a) the pool size of plant available N based on a better understanding of various N pools and fluxes, (b) NPP and decomposition based on the revised N availability, and (c) N_2O emissions such that the whole budget of peatland greenhouse gas (GHG) emissions can be derived.

2.3. Model Simulation and Post-Processing

The model was parameterized in terms of (a) the soil C:N ratio determining the balance between mineralization and immobilization, and (b) the spatially explicit monthly maximum C assimilated by the ecosystem. The parameterization method is provided Text S2 in Supporting Information S1. The historical model input (15 ka BP-1990) was derived from TraCE 21ka dataset (He, 2011) and the future inputs were derived from two CMIP5 products: IPSL-CM5A-LR and bcc-csm1-1, covering three warming scenarios: RCP 2.6, RCP 4.5 and RCP 8.5. Among many CMIP5 data products, the IPSL-CM5A-LR dataset shows low biases when compared to the historical data in Eurasia and North America (Miao et al., 2014; Sheffield et al., 2013). However, IPSL-CM5A-LR predicts extreme warming in RCP 8.5, thereby the bcc-csm1-1 dataset was also selected as a milder projection. The climate projections of these two models were able to cover a range of CMIP5 models (Miao et al., 2014; Palmer et al., 2018). A simulation was conducted with both forcings by PTEM 2.2, which has been implemented with the limited N cycle. The previous simulation, conducted until 2300, used both CMIP5 datasets, chosen for their coverage until 2300 and three warming scenarios. In this study, we used the same forcing for a revised PTEM 2.3 to ensure that the role of the N cycle can be analyzed by comparing the two simulations. Both the historical (15 ka BP-1990) and two CMIP5 forcings (1990–2100) were corrected by the CRU dataset. The processing of the historical and future model inputs is documented Text S3 in Supporting Information S1. The correction of CMIP5 forcing ensures that the differences in future C and N dynamics are derived from the different levels of warming in the future but not the difference in these forcings in the past.

In order to estimate the C and N dynamics of northern peatlands during 15 ka BP-2100, three sets of simulations were conducted:

1. WTD simulation: PTEM 2.3 was first used to simulate the WTD of each grid cell from 15 ka BP to 2100. This simulation was conducted six times–twice for each set of future CMIP5 forcing, corresponding to three warming scenarios. In consistent with PTEM 2.2, the simulated grid cell WTD was used to estimate the dynamic wetland WTD via a TOPMODEL approach. Notably, in this study, peatland extent during 1990–2100 was assumed to be constant for two reasons: First, PTEM 2.2 simulation indicated less than 0.1Mkm^2 change in peatland area during 1990–2100 (Zhao & Zhuang, 2023). Second, projecting peatland area change requires simulation of millions of bins, which consumes a significant amount of computational resources. As peatland area change was not considered, the spatially explicit wetland WTD was estimated from the averaged TWI of all wetland bins in each grid cell. This simplification reduced the number of simulations from the number of bins (millions) to the number of grid cells (around 25,000).

Table 1
Pan-Arctic Peatlands C Sink Capability and Its Sensitivity to Climate

Model	RCP 2.6	R^2	RCP 4.5	R^2	RCP 8.5	R^2
Pan-Arctic peatlands C sink capability increases (Tg C·yr^{-1}) in response to 1°C annual temperature increase						
IPSL-CM5A-LR	−28.2	0.53	−34.6	0.76	−48.9	0.92
bcc-csm1-1	−18.1	0.13	−14.6	0.18	−32.5	0.76
Annual temperature threshold of C sink-source conversion						
IPSL-CM5A-LR	−1.8	0.19	−2.2	0.71	−2.0	0.67
bcc-csm1-1	4.4	0.01	0.6	0.08	−0.5	0.60
Annual precipitation threshold of C sink-source conversion						
IPSL-CM5A-LR	496.5	0.16	487.2	0.57	490.4	0.64
bcc-csm1-1	682.8	0.00	529.3	0.13	507.6	0.58
Annual unfrozen day threshold of C sink-source conversion						
IPSL-CM5A-LR	192	0.62	193	0.89	211	0.76
bcc-csm1-1	−[a]	−[a]	219	0.50	213	0.87
Annual precipitation increase (mm) in response to 1°C annual temperature increase						
IPSL-CM5A-LR	12.7	0.58	13.3	0.82	12.0	0.92
bcc-csm1-1	13.4	0.37	14.3	0.66	13.6	0.89

[a]An effective threshold can not be identified.

2. Preliminary PTEM 2.3 simulation: the wetland WTD derived from step 1 was used as an input to this simulation. This simulation was conducted only once for the past (15 ka BP-1990). The output gives information on the spatially explicit final peat thickness n (cm) in 1990 and the year i (BP) when peat thickness first exceeds a given value m (cm, $m = 0, 1, 2, \ldots n$). In an earlier study, we established a pan-Arctic peat expansion trend from observation records, that is, the relationship between year i (BP) and relative peatland abundance A (0 in 15 ka BP and 1 in 1990) (Zhao, Zhuang, & Frolking, 2022). This trend was assumed to be applicable to each pan-Arctic grid cell; therefore, a spatially explicit peat expansion trend until 1990 can be described by the relationship between m (cm, $m = 0, 1, 2, \ldots n$) and A (0–1) (Zhao, Zhuang, & Frolking, 2022).

3. Final PTEM 2.3 simulation: the spatially explicit peat expansion trend from step 2 and wetland WTD from step 1 were both inputs to this simulation. This simulation was conducted six times covering 15ka BP-2100.

The simulation results of step 3 were analyzed in terms of (a) historical C and N accumulation and GHG emissions; (b) future organic and mineral N dynamics and their impact on C dynamics; (c) future GHG emissions and C budget; (d) the threshold temperature and precipitation when northern peatlands' likelihood of being a net C source is greater than 0.5. The threshold temperature and precipitation were calculated using the same method as the PTEM 2.2 simulation (Zhao & Zhuang, 2023a). Table 1 provides the threshold calculated from forcing data and model outputs during 1990–2100, while Table S3 in Supporting Information S1 provides the result from long-term forcing and outputs, that is, 15 ka BP-2100.

The radiative forcing (RF) of peatlands GHG fluxes was calculated to evaluate the effect of northern peatlands on climate. The estimation of RF was derived from the impulse-response model designed for peatlands (Dommain et al., 2018). This model divides CO_2 fluxes into five pools by their lifetime, and CH_4 fluxes are treated as a whole pool. The atmospheric perturbation due to GHG flux is calculated by the annual net GHG emission, the lifetime of GHG in each pool and the fraction of each pool in total flux. In addition, in order to convert from atmospheric perturbation to RF, the GHG's radiative efficiency (W m^{-2} ppb^{-1}), an indirect multiplier of GHG and the converter between GHG emissions (Tg) to ppb are required. These parameters are given for the CO_2 and CH_4 pools but not the N_2O pool (Dommain et al., 2018). Therefore, we assumed N_2O flux to be an entire pool. The N_2O parameters such as lifetime (121 years), radiative efficiency (3×10^{-3} W m^{-2} ppb^{-1}), and the indirect effect multiplier (1) are given in Myhre et al. (2013). The unit converter is 7.65 Tg N_2O per ppb, as derived from Denman et al. (2007). Notably, the RF estimated by the impulse-response model describes the cumulative effect of peatlands on climate since 15 ka BP. The RF in a year is not only influenced by the newly released/absorbed GHG but also by the long-term balance of CO_2 fluxes. Therefore, in a year when the peatlands temporarily act as a net eCO_2 emitter, they could still have a negative RF due to the remaining cooling effect of the previous absorbed CO_2.

3. Results

3.1. Holocene N Dynamics

The total N stock in northern peatlands is controlled by four N fluxes: N fixation, N deposition, N gas emission and N loss through water flow (Figure 2a). In particular, the N flux through BNF, deposition and gas emission are stable through the Holocene, with an average rate of 0.80 ± 0.09 gN m^{-2} yr^{-1}, 0.69 ± 0.09 gN m^{-2} yr^{-1} and 0.24 ± 0.06 gN m^{-2} yr^{-1}, respectively. On average, the water flow carries more N out than carrying in, and the N loss rate through water flow shows a slight increase trend until around 6 ka BP then stabilizes. This indicates the expansion of the mineral N pool size at the regional scale and the stabilization after around 6 ka BP, that is, the
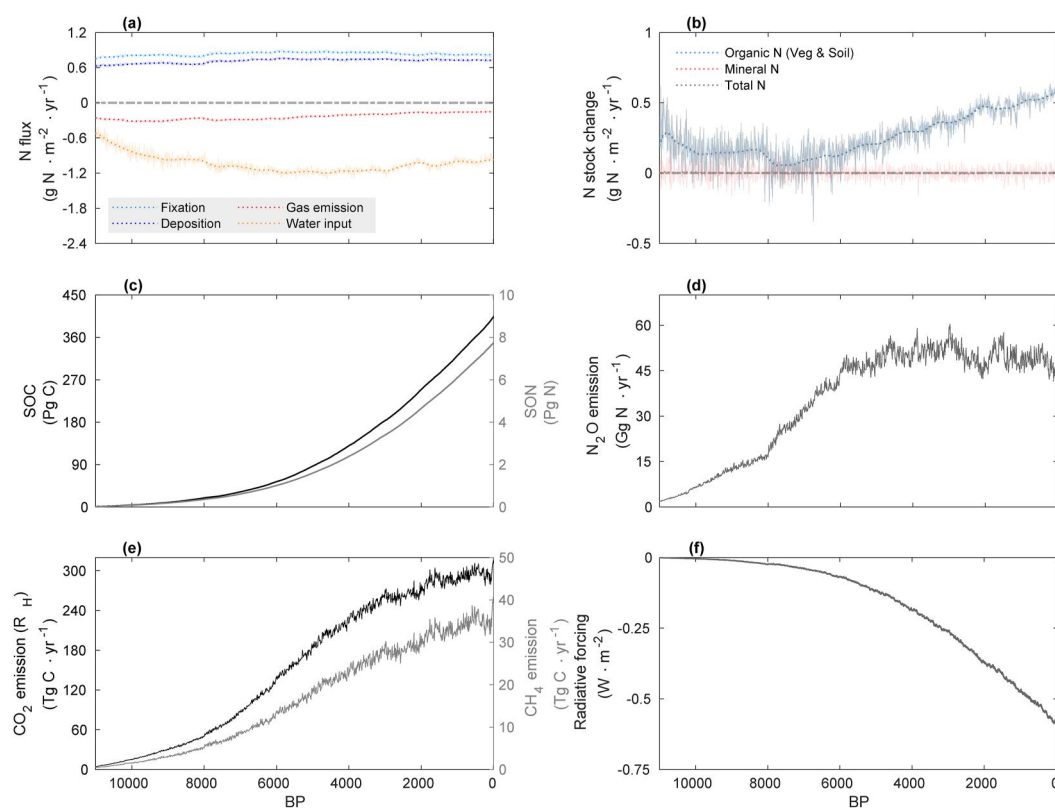
Figure 2. Time series of (a) N fluxes through BNF, deposition, gas emission and water flow; (b) changes in organic, mineral and total N stock; (c) soil organic C and organic N stock; (d) regional N2O emission; (e) regional soil heterotrophic respiration (RH) and CH4 emission; (f) the radiative forcing of northern peatlands.

rates of mineral N flowing in and out of the ecosystem are similar since then. The long-term N loss via water flow is 0.91 ± 0.27 gN m^{-2} yr^{-1}.

Although all these N fluxes are inorganic, the input N is mostly converted to and stored as organic matter (both vegetation and soil, Figure 2b). In particular, mineral N is converted into organic N via vegetation N uptake, and the reverse process is the positive net N mineralization (Figures S3a and S3b in Supporting Information S1). Since the vegetation N uptake rate is generally higher than the net N mineralization rate (1.53 ± 0.20 vs. 1.08 ± 0.28 gN m^{-2} yr^{-1}), a net conversion from mineral to organic N is simulated. Furthermore, the vegetation N uptake rate and litter N fall rate are close, indicating that most of the system input N is transferred from the vegetation N pool to the soil organic N pool (Figure S3c in Supporting Information S1). Therefore, the total N pool size depends on the soil organic N amount that is determined by the input (i.e., litterfall N) and output (i.e., conversion to mineral N). With higher temperature and precipitation, more organic N is converted to mineral form, leading to higher plant-available mineral N, and thereby higher plant N uptake. As a result, the trends of net N mineralization, vegetation N uptake and litterfall N are highly consistent with each other (Figures S3 and S4 in Supporting Information S1). Since litterfalls tend to override net N mineralization in our simulation, a continuous increase in the soil organic N is found (Figure 2b), this increase is faster when litterfall N increases faster than net N mineralization rate, and vice versa. As a result, a slower N stock increase is simulated around 8ka BP and recovered since 7 ka BP (Figure 2b).

Although the simulation starts in 15 ka BP, the major increase in SON stock is not found until 11–12 ka BP (Figure 2c). The estimated soil organic N stock is 7.8 Pg. On a 500-year bin basis, the pan-Arctic peatlands N accumulation rate (NAR) range is 0.25–0.54 gN m^{-2} yr^{-1}, and the long-term NAR is 0.45 gN m^{-2} yr^{-1}. The 500-year NAR on a unit area from 10 ka BP to 2 ka BP generally decreases, while the regional SON accumulation stock accelerates. The discrepancy indicates that the accelerating SON stock change is primarily driven by the regional peatland expansion.
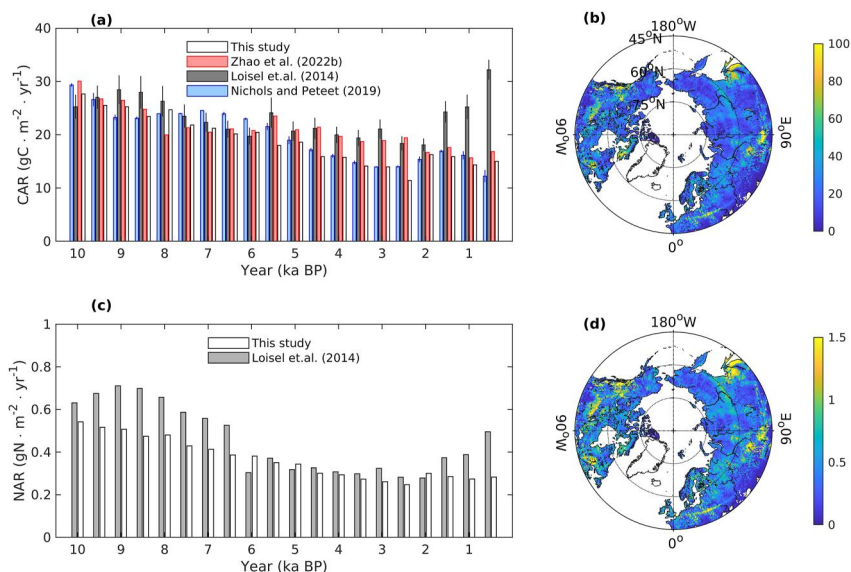
Figure 3. (a) Comparison of 500-year C accumulation rate (CAR) between this study and Loisel et al. (2014), Nichols and Peteet (2019) and Zhao, Zhuang, and Frolking (2022). (b) Spatially explicit long-term CAR per unit peatland area (gC m^{-2} yr^{-1}). (c) Comparison of 500-year N accumulation rate (NAR) between this study and Loisel et al. (2014). (b) Spatially explicit long-term NAR per unit peatland area (gN m^{-2} yr^{-1}).

3.2. Holocene C Dynamics and the Radiative Forcing

The temporal trend of SOC is consistent with that of SON (Figure 2c). The estimated soil organic C stock is 408 Pg C. Since the soil N stock is predominantly organics, the C:N ratio can be approximated by the organic C: organic N ratio, which is 52.26. On a 500-year bin basis, the pan-Arctic peatlands C accumulation rate (CAR) range is 11.40–27.65 gC m^{-2} yr^{-1}, and the long-term CAR is 23.43 gC m^{-2} yr^{-1}. Consistent with the temporal trend of SON, the accelerating SOC stock change during 10-2 ka BP is also driven by the regional peatland expansion. The hotspots of C and N accumulations are spatially consistent (Figures 3b and 3d).

As soil C and N accumulate in northern peatlands, the GHG emissions increase simultaneously (Figures 2d and 2e). Notably, N_2O emissions are influenced by the mineral N stock on the unit area basis. The mineral N pool size on the unit area basis increases before 8ka BP, stabilizes during 8-6 ka BP and decreases slightly after 6 ka BP (Figure S5 in Supporting Information S1). Meanwhile, the northern peatlands expand. As a result, N_2O emissions increase until around 6 ka BP and stabilize afterward. During the Holocene, northern peatlands always act as a C sink and have a net cooling effect on the global climate (Figure 2f). This cooling effect amplifies as more C is sequestrated into the soil. In particular, the cooling effect is mainly driven by net ecosystem exchange (i.e., NEE, net CO_2 uptake), with CH_4 emissions having warming effects and N_2O emissions having minor warming effects (Figure S6 in Supporting Information S1). Notably, a rapid increase in the GHG emission rate is simulated since around 1870 (Figure S7 in Supporting Information S1). After over 100 years of increasing, by 1990, the simulated regional N_2O, soil heterotrophic respiration (R_H) and CH_4 emissions are 56.30 GgN yr^{-1}, 327.35 TgC yr^{-1} and 47.97 TgC yr^{-1}, respectively. Due to the increase in cumulative C sequestration, northern peatlands show slightly increased RF, reaching −0.57 W m^{-2} by 1990.

3.3. N Fluxes, N Stocks and the Influence on NPP During 1990–2100

As the climate warms, all N fluxes are more intensive, with the N loss via water flow increasing more than the other pathways (Figure 4). Under the RCP 2.6, northern peatlands are a N sink. Under the RCP 4.5, northern peatlands maintain an N sink with bcc-csm1-1 forcing, and switch from a sink to N neutral with IPSL-CM5A-LR forcing. Under the RCP 8.5, northern peatlands switch from a sink to a N source under both forcing. Notably, in all scenarios, the mineral N stock is consistently increasing (Figure 4, Table S2 in Supporting Information S1). On the contrary, the organic N stock switches from a sink to nearly N neutral under the RCP 2.6 and switches to a source under the RCP 4.5 and RCP 8.5. This is the result of the overall higher increase in net N mineralization rate
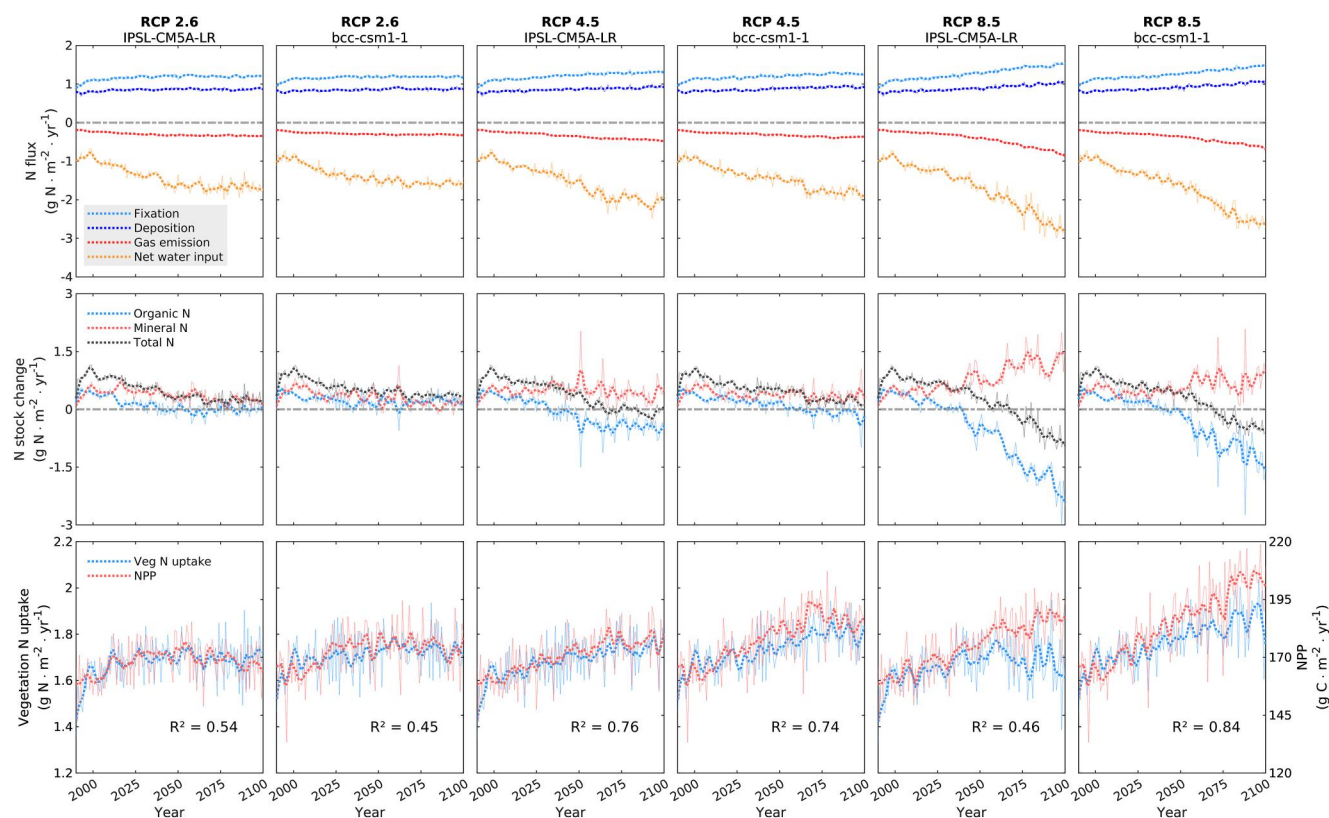
Figure 4. Time series of N fluxes (top panel), changes in organic and mineral N stocks (middle panel) and vegetation N uptake and net primary productivity (bottom panel) during 1990–2100.

than vegetation N uptake rate (Figure S11 in Supporting Information S1, Figure 4). Therefore, peat soil is generally mineralized under warming. In particular, during 2000–2100, the organic N stock increases by 0.1 Pg N under the RCP 2.6, 0–0.1 Pg N under the RCP 4.5, and decreases by 0.1–0.2 Pg N under the RCP 8.5. In addition, the warmer lower latitude regions first show organic N loss (Figures S12 and S13 in Supporting Information S1). However, the mineral N stock keeps increasing under all warming scenarios by 0.1, 0.1–0.2 and 0.2–0.3 Pg N under the RCP 2.6, RCP 4.5 and RCP 8.5, respectively (Table S2 and Figure S14 in Supporting Information S1). As a result, the total N pool increases by 0.1–0.2 Pg N under all scenarios, with hotspots in eastern Eurasia and North America arctic (Figures S15 and S16 in Supporting Information S1). Under the expanded mineral N pool and higher temperature, we estimate that during the 21st century, N_2O emissions will increase by 30.5–37.4, 48.6–95.7 and 189.3–277.8 Gg N yr^{-1} under the RCP 2.6, RCP 4.5 and RCP 8.5, respectively (Table S2 and Figure S14 in Supporting Information S1). However, the contribution of N_2O emissions to future warming is minor due to the relatively small amount (Figure S22 in Supporting Information S1).

3.4. C Fluxes, C Stocks and the Radiative Forcing During 1990–2100

With the warmer climate and higher mineral N content, the vegetation N uptake increases, thereby stimulating NPP (Figure 4 and Figure S17 in Supporting Information S1). The correlation coefficient (R^2) between N uptake and NPP is 0.45–0.84, depending on the warming scenario (Figure 4). During 2000–2100, regional NPP increases by 12–33.6, 57.7–62.9 and 86.5–100.1 TgC yr^{-1} under the RCP 2.6, RCP 4.5 and RCP 8.5, respectively (Table S2 in Supporting Information S1).

As C sequestration increases, the C emissions are also more intense (Figure 5). From 2000 to 2100, under the RCP 2.6, RCP 4.5 and RCP 8.5, R_H increases by 38.9–59.5, 71.0–160.6 and 281.4–351.4 TgC yr^{-1}, respectively, while the increase of CH_4 emissions is 8.9–11.7, 19.0–42.2 and 101.5–142.3 TgC yr^{-1}, respectively (Table S2 in Supporting Information S1). With more NPP increase than C emissions, northern peatlands maintain as a C sink until at least 2100 under the RCP 2.6 with both forcing, and the RCP 4.5 with bcc-csm1-1 forcing. The opposite
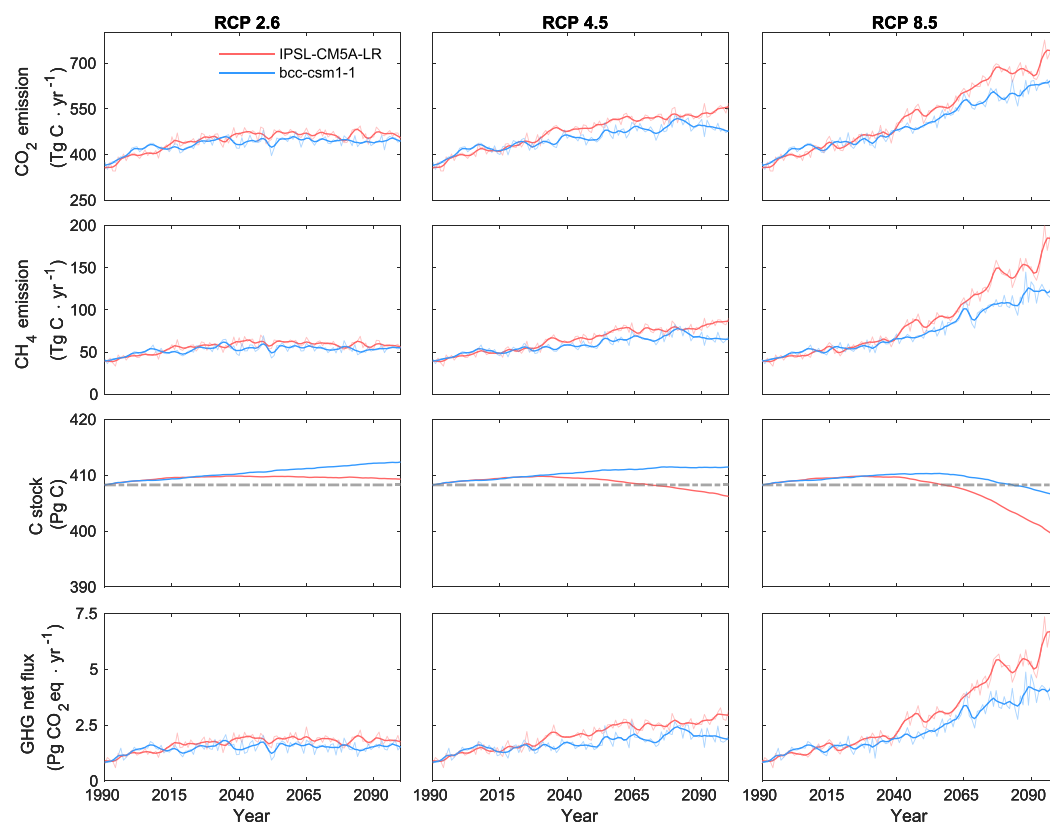
Figure 5. Time series of soil heterotrophic respiration (R_H), CH_4 emissions, C stock and radiative forcing of northern peatlands during 1990–2100.

trend is found under the other three warming scenarios (i.e., IPSL-CM5A-LR + RCP 4.5, IPSL-CM5A-LR + RCP 8.5 and bcc-csm1-1 + RCP 8.5), where northern peatlands become a C source of 2.7, 10.3 and 2.7 Pg C, respectively (Figure 5, Table S2 in Supporting Information S1).

We estimate that with 1°C annual temperature increase, the northern peatlands C sink capability decreases by 14.6–48.9 TgC yr^{-1}, and the correlation is better when warming is severe (Table 1). With a 1°C annual temperature increase, the precipitation under IPSL-CM5A-LR increases less than under bcc-csm1-1, while the opposite is found in C sink capacity (Table 1). This indicates that peatland C sink capacity prefers high-moisture conditions.

We calculated the threshold temperature, precipitation and unfrozen day number to shift a C sink to a source for northern peatlands. Relatively high R^2 values exist only when persistent sink to source conversion happens (i.e., IPSL-CM5A-LR + RCP 4.5, IPSL-CM5A-LR + RCP 8.5 and bcc-csm1-1 + RCP 8.5). Under these three scenarios, when calculating only from the forcings and the model outputs during the 21st century, the threshold temperature is −2.2 to −0.5°C, the threshold precipitation is 487.2–507.6 mm•yr^{-1}, and the threshold unfrozen day number is 193–213 (Table 1). When northern peatlands occasionally act as a C source shortly before the 21st century, the threshold temperature and precipitation are also calculated from the long-term forcings and the model outputs during 15ka BP-2100. The thresholds are similar to the temperature of −2.2 to −0.1°C, and the precipitation of 487.2–524.4 mm yr^{-1} (Table S3 in Supporting Information S1).

Under all scenarios, the RF of northern peatlands remains negative, indicating a cooling effect persists despite the warming background (Figure 5). During 2000–2100, the northern peatlands RF increases by 0.1, 0.1–0.2 and 0.3–0.5 W m^{-2} under the RCP 2.6, RCP 4.5 and RCP 8.5, respectively (Table S2 in Supporting Information S1), indicating there is a reduced negative effect of northern peatlands on future warming. Under all scenarios, the RF derived from CO_2 flux is stable and N_2O emissions have minor effects on the total RF (Figure S22 and Table S4 in Supporting Information S1). Therefore, the increase in RF is mainly driven by the higher emissions of CH_4, which

has a shorter lifetime (Myhre et al., 2013) and responds to the climate change swiftly (Figure S22 in Supporting Information S1). In particular, the RF derived from CH_4 emissions contributes to 93%–100% of RF increase during 2000–2050%, and 90%–99% of RF increase during 2050–2100 (Table S4 in Supporting Information S1).

4. Discussion

4.1. Holocene C and N Dynamics

By 1990, our simulated northern peatlands soil C stock is close to the estimation from PTEM 2.1 (408 Pg C vs. 404 Pg C) (Zhao, Zhuang, & Frolking, 2022), Qiu et al. (2019) (408 Pg C) and Hugelius et al. (2020) (400 Pg C). The estimated soil organic N stock (7.8 Pg N) is within the range of 10 ± 7 Pg N reported by Hugelius et al. (2020). Our estimated soil C:N ratio is slightly lower than the values from Loisel et al. (2014) (52.3 vs. 55 ± 33) and higher than the values from Hugelius et al. (2020) (52.3 vs. 41.5). Notably, the simulated C:N ratio has a much smaller standard deviation compared to the values from Loisel et al. (2014) (8.4 vs. 33). As the peats' C:N ratio highly varies by their botanical origin (Loisel et al., 2014), this difference indicates that the PFT variation in the observation could be higher than in the simulation.

The long-term CAR of pan-Arctic peatlands is similar to the estimation from PTEM 2.1 (23.43 gC m^{-2} yr^{-1} vs. 22.9 gC m^{-2} yr^{-1}) (Zhao, Zhuang, & Frolking, 2022), and agrees with the observed or simulated values from the literature (17.3–26.1 gC m^{-2} yr^{-1}) (Chaudhary et al., 2020; Loisel et al., 2014; Turunen et al., 2002; Yu et al., 2009). The temporal trend of 500-year CAR from this study is generally consistent with Loisel et al. (2014), Nichols and Peteet (2019) and Zhao, Zhuang, and Frolking (2022) (Figure 3). In the PTEM 2.1 simulation (Zhao, Zhuang, & Frolking, 2022), where a complete N cycle was not considered and the wetland WTD was not derived from TOPMODEL, the simulation result was closer to Loisel et al. (2014). However, in this study, the simulated CAR is closer to Nichols and Peteet (2019). The temporal trend of 500-year NAR is consistent with Loisel et al. (2014), and the long-term NAR is close (0.45 gN m^{-2} yr^{-1} vs. 0.5 ± 0.04 gN m^{-2} yr^{-1}) (Figures 3a and 3c).

The cooling effect of northern peatlands amplifies as more C is sequestered into the soil, which is consistent with previous studies (Dommain et al., 2018; Frolking & Roulet, 2007). Our estimated RF by 1990 (-0.57 W m^{-2}) is close to -0.2 to -0.5 W m^{-2} estimated by Frolking and Roulet (2007). The discrepancy could be due to the divergent peatlands C pool estimates between these models and the differences in the impulse-response model parameters used to calculate RF (Dommain et al., 2018).

4.2. N Dynamics Under Future Warming

Our estimated BNF during 2010–2020 (0–2.88 gN m^{-2} yr^{-1}, with an average of 1.12 gN m^{-2} yr^{-1}) is close to the observed range during the same period (0.01–3.5 gN m^{-2} yr^{-1}) (Patova et al., 2020; van den Elzen et al., 2020).

Our estimation of recent N_2O emissions is supported by the literature. In particular, during 2009–2013, observations of N_2O emissions have a range of 0–3.1 gN·m^{-2} (Audet et al., 2013; Dinsmore et al., 2009), while our estimated N_2O emission rate is 0–2.88 gN m^{-2} yr^{-1}. At regional scales, N_2O emissions are estimated to be 30–100 Gg N yr^{-1} in the early 1990s, while our estimation is 58.63–61.35 Gg N yr^{-1} during the same period (Martikainen et al., 1993). Our estimated N_2O emissions increase as the mineral N pool expands (Figure S14 and Table S2 in Supporting Information S1). Consistent with this study, Gong et al. (2019) suggests that warming alone has limited effect on the N_2O emissions in boreal peatlands, while more abundant mineral N content could increase N_2O emissions. Similarly, N_2O emissions are reported to peak after N fertilization in Swedish bogs (Lund et al., 2009). In addition, permafrost thaw (i.e. reduced permafrost area and deepening ALD, Figures S8–S10 and Table S2 in Supporting Information S1) is simulated during warming, leading to a higher amount of N taking part in nitrification and denitrification, and benefits N_2O emissions (Voigt et al., 2020). However, both this study and Hugelius et al. (2020) find a minor contribution of N_2O emissions to the future RF variation.

4.3. Effects of N Cycling on Future C Dynamics

Compared with the PTEM 2.2 simulation with no complete N cycle, this study projects higher NPP in the future (Zhao & Zhuang, 2023a). Both studies use the same forcings and N limiting effects on productivity algorithms. Therefore, this difference in NPP should be attributed to the higher N availability in this study. In other words, adding the N fluxes via fixation, deposition, gas emission, and water transportation to the model eventually expands the available mineral N pool size under the warming climate. An indirect effect of more abundant N is

that higher NPP stimulates CH_4 emissions (Zhao, Zhuang, Treat, & Frolking, 2022). Compared with PTEM 2.2 (Zhao & Zhuang, 2023a), the CH_4 emissions by 2100 are higher in this study by 12.8–68.0 TgC yr^{-1}. Notably, the increase in CH_4 emissions is not solely due to the higher productivity but also driven by the effect of WTD dynamics and temperature increase. Previous simulations indicate that northern peatlands WTD will be deeper during the 21st century, which has a negative effect on CH_4 emissions (Evans et al., 2021; Zhao & Zhuang, 2023a). However, our results indicate that the positive effect of warming and NPP will override the negative effect of deeper WTD, and thereby CH_4 emissions will still increase.

Compared with the previous simulation (Zhao & Zhuang, 2023a) with both forcings, the CAR in the 21st century is consistently higher in this simulation with the N cycle (Figures S20 and S21 in Supporting Information S1). In particular, in the higher latitudes, the CAR with the N cycle is higher, while the opposite is found in the lower latitude region. Since the region with higher peatland abundance tends to have higher CAR with the N cycle, the N cycle increases regional average CAR by 2.5–16.3 gC m^{-2} yr^{-1}. As the climate warms up in the late 21st century, the delta CAR becomes higher, indicating the increasing importance of the N cycle under future warming in C cycling (Figures S20 and S21 in Supporting Information S1). Under the effect of N cycling, this study projects that there is a higher threshold temperature determining northern peatlands C sink-source conversion (−2.2 to −0.5°C vs. −2.9 and −2.1°C), and the projected conversion is delayed (Zhao & Zhuang, 2023a).

4.4. C Dynamics and Radiative Forcing Under Warming

Future CO_2 emissions increase because of the higher temperature, WTD drawdown and PFT shift. In particular, the expansion of woody plants, which are more susceptible to decomposition, is simulated by PTEM 2.2 as WTD draws down in the 21st century (Zhao & Zhuang, 2023a). As the future WTD in PTEM 2.2 and 2.3 is simulated by the same technical routine, and the influence of WTD on PFT dominance is the same, these explanations of CO_2 emissions increase in PTEM 2.2 are also applicable to PTEM 2.3.

We project that northern peatlands remain C sinks under milder warming scenarios but will convert to sources under relatively severe warming (Figure 5, Table S2 in Supporting Information S1). This projection agrees with the result from Qiu et al. (2020). Under all scenarios, the warmer climate (i.e., higher temperature and precipitation) linearly correlates with less C sink capability of pan-Arctic peatlands (Table 1). Therefore, as the temperature increases, CAR generally decreases. Similarly, Chaudhary et al. (2020) estimate lower CAR as the temperature increases, while the northern peatlands are still C sinks until 2100 under the RCP 8.5 in their study.

Our simulated results indicate that the warmer lower latitude regions first switch to C sources (Figures S18 and S19 in Supporting Information S1). Similarly, Gallego-Sala et al. (2018) project that with the increases in respiration overriding the increases in productivity, lower-latitude northern peatlands first switch to a net C source. In addition, the permafrost southern boundary is more vulnerable to thawing, as suggested by our study (Figures S9 and S10 in Supporting Information S1) and Hugelius et al. (2020). In PTEM, when permafrost thaws or degrads in the southern boundary, the previously frozen peat starts to decompose. However, the C loss via SOC dissolving and outflowing is not considered in PTEM 2.3, which is argued to be a significant C loss pathway for permafrost peatlands (Hugelius et al. (2020).

This study chooses 15 ka BP as the start point of RF calculation. As a result, the RF in 2100 remains negative (Figure 5). This is different from the common approach of choosing 1750 CE as the starting point, in which case the post-industrialization RF is positive (Forster et al., 2007). Despite the difference in methods and values, this study finds RF being relatively stable during 1750–1870 CE and starting to increase since 1870 CE, which remains consistent with the literature (Myhre et al., 2013).

This study emphasizes the predominant role of CH_4 emissions in the future RF. In agreement with this study, Qiu et al. (2021) project an increased warming effect from CH_4 emissions during 1990–2100. Similarly, Hugelius et al. (2020) suggest that the main driver of GHG forcing is CH_4 emissions under warming and the permafrost thaw. At the site level, CH_4 emissions account for 60%–85% of the total CO_2 equivalent emissions in a drained coastal wetland (Gatland et al., 2014). Notably, revising the N cycle of PTEM increases CH_4 emissions in 2100 by 30%–59% (Zhao & Zhuang, 2023). This result indicates a significant influence of the N cycle on northern peatlands' future response to the warming climate.

4.5. Uncertainty Sources and Limitations of PTEM 2.3

The first uncertainty source of PTEM 2.3 in simulating regional N fluxes is from BNF. Until now, the mechanisms of northern peatlands BNF are still not well-understood (Yin et al., 2022). The inadequate number of BNF observation limits (a) the reliability of PTEM 2.3 parameterization and (b) the comparison between the model and observations. However, BNF contributes to $31.2 \pm 2.4\%$ of total mineral N inputs during the Holocene, and $29.6 \pm 3.9\%$ and $33.1 \pm 1.2\%$ during the 21st century (Figures S23 and S24 in Supporting Information S1). As a result, the BNF-derived uncertainties significantly influence the estimation of the available N amount and NPP.

The second uncertainty source is N deposition. N deposition contributes to $27.5 \pm 6.3\%$ of total mineral N inputs during the Holocene, and $21.0 \pm 3.6\%$ and $24.2 \pm 1.3\%$ during the 21st century (Figures S23 and S24 in Supporting Information S1). PTEM 2.3 does not consider the elevated dry deposition due to human activities (Reay et al., 2008). With that considered, the mineral and available N amount will increase. Consequently, NPP will increase.

The third uncertainty source is the N flux via water flow. This process is not only influenced by the N concentration in the water but also by the run-on and runoff intensity. However, the latter is challenging to be quantified at the pan-Arctic scale. As one of the major N loss pathways ($33.3 \pm 6.3\%$ during the Holocene and $40.6 \pm 4.3\%$ and $43.5 \pm 6.5\%$ during the 21st century, Figures S23 and S24 in Supporting Information S1), the underestimation of run-on or the overestimation of runoff will cause the underestimation of the available N pool, and vice versa.

All the listed uncertainties influence the estimation of N_2O emissions indirectly by changing the amount of mineral N (Gong et al., 2019). N gas loss contributes to $8.9 \pm 2.0\%$ of the total mineral N loss during the Holocene, and $8.5 \pm 0.5\%$ and $10.8 \pm 2.5\%$ during the 21st century (Figures S23 and S24 in Supporting Information S1). If there is an overestimation of N_2O emissions, both N gas loss and RF will increase, and vice versa.

Three major limitations of PTEM 2.3 are identified. First, PTEM 2.3 does not consider disturbances such as drainage or management practices. This is different from Forest-DNDC (DeNitrification DeComposition), which has been used for wetland GHG emission estimation (Li et al., 2005). Second, both DNDC and TRIPLEX-GHG have microbial biomass pools and keep track of nitrifiers and denitrifiers in the N pools (Li et al., 2005; Zhang et al., 2017). PTEM 2.3 has simplified processes without these pools. Third, although this study emphasizes the importance of CH_4 emissions in northern peatlands' future RF, the CH_4 emission mechanism in PTEM 2.3 is still oversimplified. For example, ebullition and the detailed microbial activities that produce and consume CH_4 are not considered (Oh et al., 2020).

5. Conclusion

Northern peatlands have been a C and N sink since their initiation. A major increase in C and N stocks is simulated since 11–12 ka. By 1990, northern peatlands are simulated to store 408 Pg C organic C and 7.8 Pg N as organic N, with a soil C:N ratio of 52.26. The long-term CAR is 23.43 gC m^{-2} yr^{-1} and the long-term NAR is 0.45 gN m^{-2} yr^{-1}, both close to the observations. The N flows in and out of northern peatlands in mineral forms, while mostly converts into organic forms through plant uptake and is stored as soil organic N through plant litterfall. During the Holocene, as peat C accumulates, northern peatlands have a simulated increasing cooling effect on the global climate system, reaching -0.57 W m^{-2} by 1990.

Under climate warming, the simulated N fluxes (i.e., N deposition, N fixation, N gas loss and net N runoff) all become more intense. Meanwhile, higher net N mineralization rates are simulated under all scenarios, with a warmer climate corresponding with more net organic to mineral N conversion. Therefore, mineral N content is projected to increase under warming, which stimulates NPP. Furthermore, the N_2O emissions increase as a result of the higher mineral N content, thawing permafrost and the higher temperature.

As the projected NPP increases during warming, C emissions also increase. As a balance between NPP and C emissions, northern peatlands are projected to be a C sink under RCP 2.6 with both forcings and RCP 4.5 with bcc-csm1-1 forcing. Under the RCP 4.5 with IPSL-CM5A-LR forcing and RCP 8.5, the conversion from a C sink to a source is simulated. Northern peatlands are likely to switch to a source when the annual temperature reaches -2.2 to $-0.5°C$.

The estimated RF of northern peatlands remains negative during 1990–2100 under all scenarios. However, with the increase in GHG emissions, RF increases, and the cooling effect weakens. The increase of RF is mainly driven by the higher emission of CH_4. In comparison, the RF derived from CO_2 fluxes is relatively stable until 2100, and the RF derived from N_2O emissions is minor. Our modeling study highlights the importance of the N cycle in quantifying the C balance in northern peatlands under climate change and future CH_4 emissions from these ecosystems in affecting the climate system.

Data Availability Statement

The model codes and output data used in this manuscript can be accessed in Purdue University Research Repository Zhao and Zhuang (2023b) (https://purr.purdue.edu/publications/4241/1).

References

Audet, J., Elsgaard, L., Kjaergaard, C., Larsen, S. E., & Hoffmann, C. C. (2013). Greenhouse gas emissions from a Danish Riparian wetland before and after restoration. *Ecological Engineering*, *57*, 170–182. https://doi.org/10.1016/j.ecoleng.2013.04.021

Chaudhary, N., Miller, P. A., & Smith, B. (2017). Modelling past, present and future peatland carbon accumulation across the pan-Arctic region. *Biogeosciences*, *14*(18), 4023–4044. https://doi.org/10.5194/bg-14-4023-2017

Chaudhary, N., Westermann, S., Lamba, S., Shurpali, N., Sannel, A. B. K., Schurgers, G., et al. (2020). Modelling past and future peatland carbon dynamics across the pan-Arctic. *Global Change Biology*, *26*(7), 4119–4133. https://doi.org/10.1111/gcb.15099

Denman, K. L., Brasseur, G., Chidthaisong, A., Ciais, P., Cox, P. M., Dickinson, R. E., et al. (2007). Couplings between changes in the climate system and biogeochemistry. In S. Solomon, D. Qin, M. Manning, Z. Chen, M. Marquis, K. B. Averyt, et al. (Eds.), *Climate change 2007: The physical science basis. Contribution of working group I to the fourth assessment report of the intergovernmental panel on climate change*. Cambridge University Press.

Dinsmore, K. J., Skiba, U. M., Billett, M. F., Rees, R. M., & Drewer, J. (2009). Spatial and temporal variability in CH_4 and N_2O fluxes from a Scottish ombrotrophic peatland: Implications for modelling and up-scaling. *Soil Biology and Biochemistry*, *41*(6), 1315–1323. https://doi.org/10.1016/j.soilbio.2009.03.022

Dommain, R., Frolking, S., Jeltsch-Thömmes, A., Joos, F., Couwenberg, J., & Glaser, P. H. (2018). A radiative forcing analysis of tropical peatlands before and after their conversion to agricultural plantations. *Global Change Biology*, *24*(11), 5518–5533. https://doi.org/10.1111/gcb.14400

Evans, C. D., Peacock, M., Baird, A. J., Artz, R. R. E., Burden, A., Callaghan, N., et al. (2021). Overriding water table control on managed peatland greenhouse gas emissions. *Nature*, *593*(7860), 548–552. https://doi.org/10.1038/s41586-021-03523-1

Finger Higgens, R. A., Chipman, J. W., Lutz, D. A., Culler, L. E., Virginia, R. A., & Ogden, L. A. (2019). Changing lake dynamics indicate a drier Arctic in Western Greenland. *Journal of Geophysical Research: Biogeosciences*, *124*(4), 870–883. https://doi.org/10.1029/2018JG004879

Finlayson, C. M., & Milton, G. R. (2018). Peatlands. In C. M. Finlayson, G. R. Milton, R. C. Prentice, & N. C. Davidson (Eds.), *The Wetland Book: II: Distribution, description, and conservation* (pp. 227–244). Springer.

Forster, P., Ramaswamy, V., Artaxo, P., Berntsen, T., Betts, R., Fahey, D. W., et al. (2007). Changes in atmospheric constituents and in radiative forcing. In *Climate change 2007: The physical science basis. Contribution of Working Group I to the Fourth Assessment Report of the Intergovernmental Panel on Climate Change*. Cambridge University Press.

Frolking, S., & Roulet, N. T. (2007). Holocene radiative forcing impact of northern peatland carbon accumulation and methane emissions. *Global Change Biology*, *13*(5), 1079–1088. https://doi.org/10.1111/j.1365-2486.2007.01339.x

Frolking, S., Roulet, N. T., Tuittila, E., Bubier, J. L., Quillet, A., Talbot, J., & Richard, P. J. H. (2010). A new model of Holocene peatland net primary production, decomposition, water balance, and peat accumulation. *Earth System Dynamics*, *1*(1), 1–21. https://doi.org/10.5194/esd-1-1-2010

Frolking, S., Talbot, J., Jones, M. C., Treat, C. C., Kauffman, J. B., Tuittila, E.-S., & Roulet, N. (2011). Peatlands in the Earth's 21st century climate system. *Environmental Reviews*, *19*(NA), 371–396. https://doi.org/10.1139/a11-014

Gallego-Sala, A. V., Charman, D. J., Brewer, S., Page, S. E., Prentice, I. C., Friedlingstein, P., et al. (2018). Latitudinal limits to the predicted increase of the peatland carbon sink with warming. *Nature Climate Change*, *8*(10), 907–913. https://doi.org/10.1038/s41558-018-0271-1

Gatland, J. R., Santos, I. R., Maher, D. T., Duncan, T. M., & Erler, D. V. (2014). Carbon dioxide and methane emissions from an artificially drained coastal wetland during a flood: Implications for wetland global warming potential. *Journal of Geophysical Research: Biogeosciences*, *119*(8), 1698–1716. https://doi.org/10.1002/2013JG002544

Gong, Y., Wu, J., Vogt, J., & Le, T. B. (2019). Warming reduces the increase in N_2O emission under nitrogen fertilization in a boreal peatland. *Science of the Total Environment*, *664*, 72–78. https://doi.org/10.1016/j.scitotenv.2019.02.012

Gorham, E., Lehman, C., Dyke, A., Janssens, J., & Dyke, L. (2007). Temporal and spatial aspects of peatland initiation following deglaciation in North America. *Quaternary Science Reviews*, *26*(3), 300–311. https://doi.org/10.1016/j.quascirev.2006.08.008

Gunnarsson, U., & Rydin, H. (2000). Nitrogen fertilization reduces Sphagnum production in bog communities. *New Phytologist*, *147*(3), 527–537. https://doi.org/10.1046/j.1469-8137.2000.00717.x

Hanson, P. J., Griffiths, N. A., Iversen, C. M., Norby, R. J., Sebestyen, S. D., Phillips, J. R., et al. (2020). Rapid net carbon loss from a whole-ecosystem warmed peatland. *AGU Advances*, *1*(3), e2020AV000163. https://doi.org/10.1029/2020AV000163

He, F. (2011). *Simulating transient climate evolution of the last deglaciation with Ccsm3* (Doctor of philosophy). University of Wisconsin-Madison.

Huang, Y., Ciais, P., Luo, Y., Zhu, D., Wang, Y., Qiu, C., et al. (2021). Tradeoff of CO_2 and CH_4 emissions from global peatlands under water-table drawdown. *Nature Climate Change*, *11*(7), 618–622. https://doi.org/10.1038/s41558-021-01059-w

Hugelius, G., Loisel, J., Chadburn, S., Jackson, R. B., Jones, M., Macdonald, G., et al. (2020). Large stocks of peatland carbon and nitrogen are vulnerable to permafrost thaw. *Proceedings of the National Academy of Sciences*, *117*(34), 20438–20446. https://doi.org/10.1073/pnas.1916387117

Li, C., Trettin, C., Sun, G., Mcnulty, S., & Butterbach-Bahl, K. (2005). Modeling carbon and nitrogen biogeochemistry in forest ecosystems. Paper presented at the In *3rd International Nitrogen Conference*.

Loisel, J., Gallego-Sala, A. V., Amesbury, M. J., Magnan, G., Anshari, G., Beilman, D. W., et al. (2021). Expert assessment of future vulnerability of the global peatland carbon sink. *Nature Climate Change*, *11*(1), 70–77. https://doi.org/10.1038/s41558-020-00944-0

Loisel, J., Yu, Z., Beilman, D. W., Camill, P., Alm, J., Amesbury, M. J., et al. (2014). A database and synthesis of northern peatland soil properties and Holocene carbon and nitrogen accumulation. *The Holocene*, *24*(9), 1028–1042. https://doi.org/10.1177/0959683614538073

Lund, M., Christensen, T. R., Mastepanov, M., Lindroth, A., & Ström, L. (2009). Effects of N and P fertilization on the greenhouse gas exchange in two northern peatlands with contrasting N deposition rates. *Biogeosciences*, *6*(10), 2135–2144. https://doi.org/10.5194/bg-6-2135-2009

Martikainen, P. J., Nykänen, H., Crill, P., & Silvola, J. (1993). Effect of a lowered water table on nitrous oxide fluxes from northern peatlands. *Nature*, *366*(6450), 51–53. https://doi.org/10.1038/366051a0

Miao, C., Duan, Q., Sun, Q., Huang, Y., Kong, D., Yang, T., et al. (2014). Assessment of CMIP5 climate models and projected temperature changes over northern Eurasia. *Environmental Research Letters*, *9*(5), 055007. https://doi.org/10.1088/1748-9326/9/5/055007

Myhre, G., Shindell, D., Bréon, F.-M., Collins, W., Fuglestvedt, J., Huang, J., et al. (2013). Anthropogenic and natural radiative forcing. In *Climate change 2013: The physical science basis. Contribution of Working Group I to the Fifth Assessment Report of the Intergovernmental Panel on Climate Change*. Cambridge.

Nichols, J. E., & Peteet, D. M. (2019). Rapid expansion of northern peatlands and doubled estimate of carbon storage. *Nature Geoscience*, *12*(11), 917–921. https://doi.org/10.1038/s41561-019-0454-z

Oh, Y., Zhuang, Q., Liu, L., Welp, L. R., Lau, M. C. Y., Onstott, T. C., et al. (2020). Reduced net methane emissions due to microbial methane oxidation in a warmer Arctic. *Nature Climate Change*, *10*(4), 317–321. https://doi.org/10.1038/s41558-020-0734-z

Ojanen, P., Penttilä, T., Tolvanen, A., Hotanen, J.-P., Saarimaa, M., Nousiainen, H., & Minkkinen, K. (2019). Long-term effect of fertilization on the greenhouse gas exchange of low-productive peatland forests. *Forest Ecology and Management*, *432*, 786–798. https://doi.org/10.1016/j.foreco.2018.10.015

Palmer, M. D., Harris, G. R., & Gregory, J. M. (2018). Extending CMIP5 projections of global mean temperature change and sea level rise due to thermal expansion using a physically-based emulator. *Environmental Research Letters*, *13*(8), 084003. https://doi.org/10.1088/1748-9326/aad2e4

Patova, E. N., Sivkov, M. D., Goncharova, N. N., & Shubina, T. P. (2020). Associations between nitrogen-fixing cyanobacteria and Sphagnum mosses in floodplain bogs of the middle Taiga (European Northeast). *Theoretical and Applied Ecology*, *1*, 117–123. https://doi.org/10.25750/1995-4301-2020-1-117-123

Qiu, C., Ciais, P., Zhu, D., Guenet, B., Peng, S., Petrescu, A. M. R., et al. (2021). Large historical carbon emissions from cultivated northern peatlands. *Science Advances*, *7*(23), eabf1332. https://doi.org/10.1126/sciadv.abf1332

Qiu, C., Zhu, D., Ciais, P., Guenet, B., & Peng, S. (2020). The role of northern peatlands in the global carbon cycle for the 21st century. *Global Ecology and Biogeography*, *29*(5), 956–973. https://doi.org/10.1111/geb.13081

Qiu, C., Zhu, D., Ciais, P., Guenet, B., Peng, S., Krinner, G., et al. (2019). Modelling northern peatland area and carbon dynamics since the Holocene with the ORCHIDEE-PEAT land surface model (SVN r5488). *Geoscientific Model Development*, *12*(7), 2961–2982. https://doi.org/10.5194/gmd-12-2961-2019

Rantanen, M., Karpechko, A. Y., Lipponen, A., Nordling, K., Hyvärinen, O., Ruosteenoja, K., et al. (2022). The Arctic has warmed nearly four times faster than the globe since 1979. *Communications Earth & Environment*, *3*(1), 168. https://doi.org/10.1038/s43247-022-00498-3

Reay, D. S., Dentener, F., Smith, P., Grace, J., & Feely, R. A. (2008). Global nitrogen deposition and carbon sinks. *Nature Geoscience*, *1*(7), 430–437. https://doi.org/10.1038/ngeo230

Richardson, A. D., Hufkens, K., Milliman, T., Aubrecht, D. M., Furze, M. E., Seyednasrollah, B., et al. (2018). Ecosystem warming extends vegetation activity but heightens vulnerability to cold temperatures. *Nature*, *560*(7718), 368–371. https://doi.org/10.1038/s41586-018-0399-1

Sheffield, J., Barrett, A., Colle, B., Fernando, D., Fu, R., Geil, K., et al. (2013). North American climate in CMIP5 experiments. Part I: Evaluation of historical simulations of continental and regional climatology. *Journal of Climate*, *26*(23), 9209–9245. https://doi.org/10.1175/jcli-d-12-00592.1

Song, Y., Song, C., Ren, J., Tan, W., Jin, S., & Jiang, L. (2018). Influence of nitrogen additions on litter decomposition, nutrient dynamics, and enzymatic activity of two plant species in a peatland in Northeast China. *Science of the Total Environment*, *625*, 640–646. https://doi.org/10.1016/j.scitotenv.2017.12.311

Spahni, R., Joos, F., Stocker, B. D., Steinacher, M., & Yu, Z. C. (2013). Transient simulations of the carbon and nitrogen dynamics in northern peatlands: From the Last glacial maximum to the 21st century. *Climate of the Past*, *9*(3), 1287–1308. https://doi.org/10.5194/cp-9-1287-2013

Treat, C. C., Jones, M. C., Alder, J., Sannel, A. B. K., Camill, P., & Frolking, S. (2021). Predicted vulnerability of carbon in permafrost peatlands with future climate change and permafrost thaw in Western Canada. *Journal of Geophysical Research: Biogeosciences*, *126*(5), e2020JG005872. https://doi.org/10.1029/2020JG005872

Turunen, J., Tomppo, E., Tolonen, K., & Reinikainen, A. (2002). Estimating carbon accumulation rates of undrained mires in Finland–application to boreal and subarctic regions. *The Holocene*, *12*(1), 69–80. https://doi.org/10.1191/0959683602hl522rp

Van Den Elzen, E., Bengtsson, F., Fritz, C., Rydin, H., & Lamers, L. P. M. (2020). Variation in symbiotic N2 fixation rates among Sphagnum Mosses. *PLoS One*, *15*(2), e0228383. https://doi.org/10.1371/journal.pone.0228383

Voigt, C., Marushchak, M. E., Abbott, B. W., Biasi, C., Elberling, B., Siciliano, S. D., et al. (2020). Nitrous oxide emissions from permafrost-affected soils. *Nature Reviews Earth & Environment*, *1*(8), 420–434. https://doi.org/10.1038/s43017-020-0063-9

Xu, J., Morris, P. J., Liu, J., & Holden, J. (2018). Peatmap: Refining estimates of global peatland distribution based on a meta-analysis. *Catena*, *160*, 134–140. https://doi.org/10.1016/j.catena.2017.09.010

Xu, R. I., & Prentice, I. C. (2008). Terrestrial nitrogen cycle simulation with a dynamic global vegetation model. *Global Change Biology*, *14*(8), 1745–1764. https://doi.org/10.1111/j.1365-2486.2008.01625.x

Yin, T., Feng, M., Qiu, C., & Peng, S. (2022). Biological nitrogen fixation and nitrogen accumulation in peatlands. *Frontiers in Earth Science*, *10*. https://doi.org/10.3389/feart.2022.670867

Yu, Z., Beilman, D., & Jones, M. (2009). Sensitivity of northern peatland carbon dynamics to Holocene climate change. *Washington DC American Geophysical Union Geophysical Monograph Series*, *184*, 55–69.

Zhang, K., Peng, C., Wang, M., Zhou, X., Li, M., Wang, K., et al. (2017). Process-based Triplex-Ghg model for simulating N2o emissions from global forests and Grasslands: Model development and evaluation. *Journal of Advances in Modeling Earth Systems*, *9*(5), 2079–2102. https://doi.org/10.1002/2017MS000934

Zhao, B., & Zhuang, Q. (2023). Peatlands and their carbon dynamics in northern high latitudes from 1990 to 2300: A process-based biogeochemistry model Analysis. *Biogeosciences*, *20*(1), 251–270. https://doi.org/10.5194/bg-20-251-2023

Zhao, B., & Zhuang, Q. (2023b). Weakening cooling effect of northern peatlands on the global climate system during the 21st century [Dataset]. *Purdue University Research Repository*. https://doi.org/10.4231/BB7M-HN65

Zhao, B., Zhuang, Q., & Frolking, S. (2022). Modeling carbon accumulation and permafrost dynamics of northern peatlands since the Holocene. *Journal of Geophysical Research: Biogeosciences*, *127*(11), e2022JG007009. https://doi.org/10.1029/2022JG007009

Zhao, B., Zhuang, Q., Treat, C., & Frolking, S. (2022). A model Intercomparison Analysis for Controls on C accumulation in North American peatlands. *Journal of Geophysical Research: Biogeosciences*, *127*(5), e2021JG006762. https://doi.org/10.1029/2021JG006762

References From the Supporting Information

Anderson, D. E. (1998). A reconstruction of Holocene climatic changes from peat bogs in North-west Scotland. *Boreas*, *27*(3), 208–224. https://doi.org/10.1111/j.1502-3885.1998.tb00880.x

Andersson, S., & Schoning, K. (2010). Surface wetness and mire development during the late Holocene in Central Sweden. *Boreas*, *39*(4), 749–760. https://doi.org/10.1111/j.1502-3885.2010.00157.x

Basilier, K., Granhall, U., Stenström, T.-A., & Stenstrom, T. A. (1978). Nitrogen fixation in wet minerotrophic moss communities of a subarctic mire. *Oikos*, *31*(2), 236–246. https://doi.org/10.2307/3543568

Borken, W., Horn, M. A., Geimer, S., Aguilar, N. a. B., & Knorr, K.-H. (2016). Associative nitrogen fixation in nodules of the conifer *Lepidothamnus fonkii* (*Podocarpaceae*) inhabiting ombrotrophic bogs in southern Patagonia. *Scientific Reports*, *6*(1), 39072. https://doi.org/10.1038/srep39072

Bunbury, J., Finkelstein, S. A., & Bollmann, J. (2012). Holocene hydro-climatic change and effects on carbon accumulation inferred from a peat bog in the Attawapiskat River Watershed, Hudson Bay Lowlands, Canada. *Quaternary Research*, *78*(2), 275–284. https://doi.org/10.1016/j.yqres.2012.05.013

Camill, P., Barry, A., Williams, E., Andreassi, C., Limmer, J., & Solick, D. (2009). Climate-vegetation-fire interactions and their impact on long-term carbon dynamics in a boreal peatland landscape in northern Manitoba, Canada. *Journal of Geophysical Research*, *114*(G4). https://doi.org/10.1029/2009JG001071

Fao/Unesco. (1974). Soil map of the world.

Harris, I., Jones, P. D., Osborn, T. J., & Lister, D. H. (2014). Updated high-resolution grids of monthly climatic observations – The CRU TS3.10 dataset. *International Journal of Climatology*, *34*(3), 623–642. https://doi.org/10.1002/joc.3711

Hill, B. H., Jicha, T. M., Lehto, L. L. P., Elonen, C. M., Sebestyen, S. D., & Kolka, R. K. (2016). Comparisons of soil nitrogen mass balances for an ombrotrophic bog and a minerotrophic fen in northern Minnesota. *Science of the Total Environment*, *550*, 880–892. https://doi.org/10.1016/j.scitotenv.2016.01.178

Koerselman, W., Van Kerkhoven, M. B., & Verhoeven, J. T. (1993). Release of inorganic N, P and K in peat soils; effect of temperature, water chemistry and water level. *Biogeochemistry*, *20*(2), 63–81. https://doi.org/10.1007/BF00004135

Kokfelt, U., Reuss, N., Struyf, E., Sonesson, M., Rundgren, M., Skog, G., et al. (2010). Wetland development, permafrost history and nutrient cycling inferred from late Holocene peat and lake sediment records in subarctic Sweden. *Journal of Paleolimnology*, *44*(1), 327–342. https://doi.org/10.1007/s10933-010-9406-8

Kuhry, P., & Vitt, D. H. (1996). Fossil carbon/nitrogen ratios as a measure of peat decomposition. *Ecology*, *77*(1), 271–275. https://doi.org/10.2307/2265676

Marthews, T. R., Dadson, S. J., Lehner, B., Abele, S., & Gedney, N. (2015). High-resolution global topographic index values for use in large-scale hydrological modelling. *Hydrology and Earth System Sciences*, *19*(1), 91–104. https://doi.org/10.5194/hess-19-91-2015

Mcguire, A. D., Melillo, J. M., Joyce, L. A., Kicklighter, D. W., Grace, A. L., Moore Iii, B., & Vorosmarty, C. J. (1992). Interactions between carbon and nitrogen dynamics in estimating net primary productivity for potential vegetation in North America. *Global Biogeochemical Cycles*, *6*(2), 101–124. https://doi.org/10.1029/92GB00219

Melton, J. R., Chan, E., Millard, K., Fortier, M., Winton, R. S., Martín-López, J. M., et al. (2022). A map of global peatland extent created using machine learning (Peat-Ml). *Geoscientific Model Development Discussions*, *2022*(12), 1–44. https://doi.org/10.5194/gmd-15-4709-2022

Montes, F., Rotz, C. A., & Chaoui, H. (2009). Process modeling of ammonia volatilization from ammonium solution and manure surfaces: A review with recommended models. *Transactions of the ASABE*, *52*(5), 1707–1720. https://doi.org/10.13031/2013.29133

Oksanen, P. O., Kuhry, P., & Alekseeva, R. N. (2001). Holocene development of the rogovaya river peat plateau, European Russian Arctic. *The Holocene*, *11*(1), 25–40. https://doi.org/10.1191/095968301675477157

Robertson, G. P., & Groffman, P. (2015). Nitrogen transformations (pp. 421–446).

Sannel, A. B. K., & Kuhry, P. (2008). Long-term stability of permafrost in subarctic peat plateaus, west-central Canada. *The Holocene*, *18*(4), 589–601. https://doi.org/10.1177/0959683608089658

Sannel, A. B. K., & Kuhry, P. (2009). Holocene peat growth and decay dynamics in sub-Arctic peat plateaus, west-central Canada. *Boreas*, *38*(1), 13–24. https://doi.org/10.1111/j.1502-3885.2008.00048.x

Schwintzer, C. R. (1983). Nonsymbiotic and symbiotic nitrogen fixation in a weakly minerotrophic peatland. *American Journal of Botany*, *70*(7), 1071–1078. https://doi.org/10.1002/j.1537-2197.1983.tb07908.x

Treat, C. C., Jones, M. C., Brosius, L. S., Grosse, G., & Walter Anthony, K. M. (2016). Radiocarbon dates of peatland initiation across the northern high latitudes. https://doi.org/10.1594/PANGAEA.864101

Yu, T., & Zhuang, Q. (2020). Modeling biological nitrogen fixation in global natural terrestrial ecosystems. *Biogeosciences*, *17*(13), 3643–3657. https://doi.org/10.5194/bg-17-3643-2020

Zhuang, Q., Mcguire, A. D., O'neill, K. P., Harden, J. W., Romanovsky, V. E., & Yarie, J. (2002). Modeling soil thermal and carbon dynamics of a fire chronosequence in interior Alaska. *Journal of Geophysical Research*, *107*(D1), FFR-3. https://doi.org/10.1029/2001JD001244